

60Si2Mn 钢表面激光熔覆铁基涂层的组织及耐磨性研究

曹新娜^{1,2}, 宋路阳^{1,2}, 黄玲玲^{1,2}, 江涛¹, 张浩强¹, 汪瑞军³, 于华^{1,2*},
詹华³, 尹丹青^{1,2}, 鲍曼雨³, 龙伟民⁴, 钟素娟⁴, 纠永涛⁴

(1.河南科技大学 材料科学与工程学院, 河南 洛阳 471000; 2.龙门实验室, 河南 洛阳 471000;
3.中国农业机械化科学研究院集团有限公司, 北京 100083;
4.郑州机械研究所有限公司, 郑州 450000)

摘要: 目的 提高 60Si2Mn 钢的表面耐磨损性能。方法 采用同步送粉方式在 60Si2Mn 钢表面进行激光熔覆 X₁、X₂ 2 种铁基粉末。通过金相显微镜、场发射扫描电镜和 X 射线衍射仪, 观察和分析熔覆层的显微组织、化学元素分布及相组成, 采用显微硬度仪、多功能摩擦磨损试验机进行硬度、耐磨损性能测试。结果 2 种熔覆层均无裂纹、气孔等缺陷, 涂层内部存在大量树枝晶、等轴晶和少量沿基材表面生长的平面晶, 其中 X₁ 熔覆层的顶部区域等轴晶数量较多, 组织更细小均匀。2 种熔覆层均由相同物相 (α -Fe) 固溶体组成, 未出现明显的其他物相的衍射峰。基体 60Si2Mn 钢平均硬度约为 300HV, X₁ 熔覆层的硬度为 950~1 000HV, 平均硬度为 975HV。X₂ 熔覆层的硬度为 784~821HV, 平均硬度为 803HV。经过球-盘磨损试验后, X₁、X₂ 熔覆层以及基体的体积磨损率分别为 1.32×10^{-4} 、 1.94×10^{-4} 、 3.29×10^{-4} mm³/(N·m)。结论 2 种熔覆层的硬度和耐磨损性能均优于基体, 其中 X₁ 熔覆层的平均硬度比 X₂ 熔覆层的高约 21%, 其体积磨损率最小, 耐磨损性能更好。

关键词: 60Si2Mn 钢; 激光熔覆; 铁基粉末; 微观组织; 耐磨损性能

中图分类号: TH117 文献标志码: A 文章编号: 1001-3660(2024)07-0164-07

DOI: 10.16490/j.cnki.issn.1001-3660.2024.07.017

Microstructure and Wear Resistance of Laser Cladded Iron-based Coatings on 60Si2Mn Steel

CAO Xinna^{1,2}, SONG Luyang^{1,2}, HUANG Lingling^{1,2}, JIANG Tao¹,
ZHANG Haoqiang¹, WANG Ruijun³, YU Hua^{1,2*}, ZHAN Hua³, YIN Danqing^{1,2},
BAO Manyu³, LONG Weimin⁴, ZHONG Sujuan⁴, JIU Yongtao⁴

(1. School of Material Science and Engineering, Henan University of Science and Technology,
Henan Luoyang 471000, China; 2. Longmen Laboratory, Henan Luoyang 471000, China;

收稿日期: 2023-01-12; 修订日期: 2023-09-20

Received: 2023-01-12; Revised: 2023-09-20

基金项目: 2021 年产业基础再造和制造业高质量发展专项项目 (TC210H02X-04); 金属材料磨损控制与成型技术国家地方联合工程研究中心 2021 年开放课题 (HKDNM202104)

Fund: Special Project of Industrial Foundation Reconstruction and High-quality Development of Manufacturing Industry in 2021 (TC210H02X-04); The National Joint Engineering Research Center for Abrasion Control and Molding of Metal Materials, 2021, Open Project (HKDNM202104)

引文格式: 曹新娜, 宋路阳, 黄玲玲, 等. 60Si2Mn 钢表面激光熔覆铁基涂层的组织及耐磨性研究[J]. 表面技术, 2024, 53(7): 164-170.
CAO Xinna, SONG Luyang, HUANG Lingling, et al. Microstructure and Wear Resistance of Laser Cladded Iron-based Coatings on 60Si2Mn Steel[J]. Surface Technology, 2024, 53(7): 164-170.

*通信作者 (Corresponding author)

3. Chinese Academy of Agricultural Mechanization Sciences Group Co., Ltd., Beijing 100083, China;

4. Zhengzhou Research Institute of Mechanical Engineering Co., Ltd., Zhengzhou 450000, China)

ABSTRACT: As an advanced surface strengthening and repairing technology, laser cladding is used to prepare metallurgically bonded coatings, which has the advantages of high surface quality, low dilution rate, small heat-affected zone in the base material, and low material loss. It has been widely utilized in many fields, such as agricultural machinery, aerospace, high-speed trains, railways, and mining machinery. In this study, laser cladding technology was employed to deposit two types of iron-based coatings on the surface of 60Si2Mn steel, which was commonly used as rotary tiller blade material. The microstructure, phase structure, hardness in the bonding zone, and wear resistance of the two cladding coatings were analyzed in detail.

Both types of cladding coatings exhibited no cracks, pores, or other defects. They contained a significant number of dendritic crystals, equiaxed crystals, and a small number of planar crystals growing along the substrate surface. The different microstructures of the cladding coatings were related to the constitutional supercooling during the solidification process, which was primarily affected by the ratio of the temperature gradient (G) to the solidification rate (R). At the interface between the cladding coatings and the substrate, solidification firstly occurred with the largest temperature gradient and the slowest solidification rate. In this region, there was no significant constitutional supercooling, leading to the formation of a planar crystalline structure. As the solidification process continued, the temperature gradient decreased and the solidification rate increased. This resulted in a larger constitutional supercooling and interface instability. The microstructure changed from planar crystals to a mixture of columnar and dendritic crystals. When the solid-liquid interface approached the surface of the cladding coatings, the cooling rate was accelerated, corresponding to a smaller G/R . At this stage, the nucleation rate exceeded the growth rate of the grains, leading to the transformation of the microstructure into smaller equiaxed crystals. The X_1 cladding coating had a higher quantity of equiaxed crystals on the surface, with a finer and more uniform microstructure. This was attributed to the presence of the vanadium (V) element in X_1 powder, which could refine the grain structure and microstructure. Both types of cladding coatings exhibited diffraction peaks at the same angles (44.7° , 65.0° , 82.3°), indicating that they were composed of the same (α -Fe) solid solution.

Both types of cladding coatings exhibited higher hardness and wear resistance compared to the substrate. The substrate had an average hardness of approximately 300HV, while the X_1 cladding coating had a hardness of 950-1 000HV with an average hardness of 975HV and the X_2 cladding coating had a hardness of 784-821HV, with an average hardness of 803HV. The X_1 cladding coating had an average hardness approximately 21% higher than the X_2 cladding coating. The volume wear rates provided information about the wear resistance of the coatings. X_1 cladding coating exhibited the lowest volume wear rate among the three materials, with a value of $1.32 \times 10^{-4} \text{ mm}^3/(\text{N} \cdot \text{m})$. X_2 cladding coating had a slightly higher volume wear rate of $1.94 \times 10^{-4} \text{ mm}^3/(\text{N} \cdot \text{m})$, while the substrate material had the highest wear rate of $3.29 \times 10^{-4} \text{ mm}^3/(\text{N} \cdot \text{m})$. Therefore, the X_1 cladding coating shows the best wear resistance, indicating that it is more resistant to material loss or damage under sliding or abrasive conditions.

KEY WORDS: 60Si2Mn; laser cladding; iron-based powder; microstructure; wear resistance

农机触土部件经常在无润滑状态下与土壤中的碎石、砂砾等硬质颗粒直接接触,其工作环境复杂,易发生磨损失效。触土部件的使用寿命不长,需经常进行更换,影响耕种效率的同时造成大量金属材料浪费^[1-4]。因此采用表面强化技术来降低农机触土部件报废率、提高材料使用寿命、增强部件耐磨性受到了广泛关注。

国内外学者常采用等离子堆焊、火焰喷涂及热喷涂等技术在农机触土部件的表面制备涂层,目的均在于提高材料表面的硬度和耐磨损性能,从而提高其作业效率并减少更换成本。郝建军等^[5]采用等离子堆焊技术在 65Mn 钢表面制备了 Fe-Cr-C-V 涂层,涂层的

维氏硬度与淬火钢相比提高了 75%,磨损量降低了 67%。Benegra 等^[6]分别采用等离子堆焊和超音速火焰喷涂技术在不锈钢表面制备了 2 种涂层,发现等离子堆焊镍铝涂层的耐磨性优于超音速火焰喷涂涂层。Niranatlumpong 等^[7-8]采用超音速火焰喷涂、等离子喷涂在旋耕刀基体上分别制备了 WC-Co 涂层和 $\text{Al}_2\text{O}_3/\text{Ti}_2\text{O}_3$ 涂层,结果显示,在砂土磨损试验中,WC-Co 涂层的耐磨性更好,刀具经热喷涂 WC-Co 涂层后的磨损率仅为淬火钢的 38%。上述表面改性技术均能提高农机触土部件的耐磨性,从而延长其使用寿命。然而上述方法多存在工艺流程复杂、熔覆层稀释率高、基体变形大等缺点。激光熔覆作为一种先进的表面强

化和修复技术,能够制备出与基体产生冶金结合的涂层,具有表层质量高、稀释率低、基体热影响区小、材料损耗小等优点,广泛应用于农机、高速列车、铁路、矿山机械等多个领域^[9-13]。本文尝试采用激光熔覆技术在旋耕刀常用材料 60Si2Mn 钢的表面分别熔覆 2 种铁基粉末,并分析 2 种熔覆层的微观组织、物相结构、结合区硬度及耐磨损性能。

1 试验

1.1 材料

使用的基体材料是 60Si2Mn 钢板,其尺寸为

100 mm×100 mm×6 mm。熔覆材料分别是 X₁ 和 X₂ 2 种铁基粉末,粉末粒径为 100~270 目,其化学成分见表 1。熔覆前首先对基板表面进行打磨,去除表面氧化层,随后在 250 ℃下进行火焰预热处理,以消除残余应力并减少温度差,防止熔覆温度过高而产生开裂。

1.2 方法

激光熔覆设备由 LDF6000-100 半导体激光器、MH50II-20 型 8 轴机械手臂、PF2/2 双料斗送粉器、平台基座、气体保护系统、水冷系统、在线监测系统以及全套自动化软件控制系统组成^[14]。采用同步送粉法在基体表面熔覆粉末,具体工艺参数见表 2。

表 1 粉末化学成分

Tab.1 Chemical composition of the powder

Materials	Cr	Mn	Ni	Si	S	P	V	Mo	C	Fe
X ₁	16.62	1.37		1.5			2.9	1.52	0.25	Bal.
X ₂	16.49	0.15	1.9	0.92	0.012	0.016			0.23	Bal.

表 2 激光熔覆工艺参数

Tab.2 Laser cladding process parameters

Laser power/W	Powder feeding rate/(r·min ⁻¹)	Scanning speed/(mm·min ⁻¹)
3 800	3.0	1 500

采用电火花线切割将激光熔覆后的试样切割成 10 mm×10 mm×6 mm 的小试块,并利用砂纸和抛光机对其进行打磨、抛光处理,随后采用王水溶液对试块截面进行腐蚀。采用 Zeiss Axio Vert A1 金相显微镜观察腐蚀后熔覆层与基体结合区的微观组织。采用 JSM-7800F 场发射扫描电镜分析基体与熔覆层结合区的化学元素分布。采用 D8 Advanced X 射线衍射仪对熔覆层表面进行物相分析,衍射参数见表 3。采用 HVS-1000A 型数显显微硬度计测试熔覆层到基体的显微硬度,测试点与点之间的距离为 0.2 mm,试验载荷选用 50 g,加载时间为 15 s。采用 UMT 多功能摩擦磨损试验机对熔覆后的 2 个试样和未熔覆的基体试样进行球-盘摩擦磨损测试,对磨材料选用直径为 6.35 mm 的氮化硅球,试验参数见表 4。利用 Nano-focus 型号激光共聚焦显微镜观察磨损后试样的表面形貌,得出磨痕面积,并进行体积磨损率计算。

表 3 X 射线衍射参数

Tab.3 X-ray diffraction parameters

Target material	Tube voltage/kV	Tube current/mA	Scanning speed/((°)·min ⁻¹)	Scanning area/(°)
Cu	40	40	0.2	20-90

表 4 摩擦磨损试验参数

Tab.4 Experimental parameters of friction and wear

Load/N	Amplitude/mm	Rate/(mm·s ⁻¹)	Temperature/℃	Loading range/mm	Time/min
20	3	3	20	3	10

2 结果及分析

2.1 熔覆层宏观形貌分析

激光熔覆后 2 种涂层的宏观形貌如图 1 所示。熔覆层表面凹槽与凸起交替排布,表面平整度较差,存在凹坑,但无宏观裂纹、气孔等缺陷。对比图 1a 和图 1b 可以看出,X₂ 熔覆层的表面较光滑,X₁ 熔覆层表面存在大量熔融合金的液滴,产生这种现象的原因可能是 X₁ 粉末的润湿性能较差或粉末分解不充分。粉末分解程度与粉末粒径有关,在熔覆粉末质

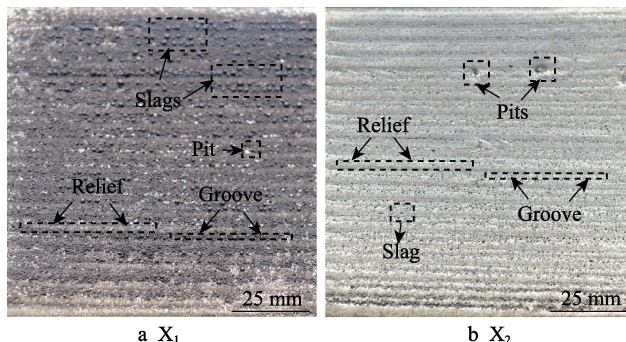


图 1 熔覆层的宏观形貌

Fig.1 Macroscopic morphologies of cladding coatings

量相同时, 粉末粒径尺寸越小, 熔化需要的能量越少, 分解程度就越高, 由此制备的熔覆层宏观形貌也更好^[15-16]。

2.2 结合区显微组织分析

图 2 为 X_1 和 X_2 2 种熔覆层的截面形貌。图 2b 和图 2e 分别为图 2a 和图 2d 界面处的局部放大, 从图中能够看到基体与熔覆层之间存在一条明显的分界线, 即熔合线。熔合线附近熔池中的金属开始结晶时, 以基体晶粒作为形核点向熔覆层中长大。激光熔覆是一个急冷急热的过程, 晶粒长大区域较小。在此生长机制下, 熔覆层和基体材料发生了元素扩散、熔合, 产生过渡区, 该区域无裂纹、气孔等缺陷。在相同腐蚀条件下, 各区域呈现的颜色有差异, 原因是各区域的耐腐蚀能力不同, 从颜色深浅可知, 熔覆层的耐腐蚀能力优于基体。图 2c 和图 2f 为 2 种熔覆层顶部区域的局部放大, 从中可以看出 X_1 熔覆层的组织更均匀、晶粒更细小。原因是 X_1 粉末中强碳化物形成元素 V 的含量较高, 易形成尺寸为纳米级的碳化物, 在晶界处严重阻碍了晶粒长大, 起到细化晶粒的作用^[17]。

熔覆层的组织形态与凝固过程中的成分过冷有关, 主要受温度梯度与凝固速率比值 (G/R) 的影响。熔覆过程中, 熔覆层与基体的结合处最先凝固, 温度梯度最大, 凝固速度最小, 故 G/R 最大, 不存在成分过冷, 凝固过程中释放的热量全部向基体界面传递, 界面处形核速度小于晶粒生长速度, 固液界面向前缓慢推进, 形成平面晶组织; 随凝固过程继续进行, 固液界面向熔覆层表面持续推进, 温度梯度持续减小, 凝固速度持续增加, G/R 逐渐减小, 造成较大的成分

过冷, 界面失稳, 组织向柱状晶或树枝晶转变; 当固液界面推进到接近熔覆层表面时, 与外界空气接触, 散热速度快, 此时 G/R 很小, 晶粒形核速度大于生长速度, 使得组织向细小的等轴晶转变^[18-22]。

2.3 熔覆层物相结构分析

图 3 为 X_1 和 X_2 2 种熔覆层与基体结合区的微观形貌和元素分布曲线。从元素分布曲线可以看出, 2 种试样中 Si、Mn、C 元素含量在基体和熔覆层中无明显变化; Fe 元素在基体中含量较多, 由基体到熔覆层含量逐渐减少, 在界面结合处元素分布发生突变; Cr 元素在熔覆层中含量较高, 由熔覆层表面向基体元素含量呈下降趋势, 元素含量在界面处变化明显。 X_1 熔覆层中存在 V 元素, 图中 V 元素的局部信号强度高于 Cr 元素。原因是 V 元素形成碳化物的能力高于 Cr 元素, 局部形成少量碳化物, 使得成分分布不均匀。相较于 X_1 熔覆层的线扫描结果, X_2 熔覆层中 Cr 元素含量相对更高, 元素含量在界面结合处的变化更明显。Cr 元素含量不仅影响熔覆层的硬度, 也影响熔覆层的耐蚀性能, 随 Cr 元素含量增加, 熔覆层硬度降低, 耐蚀性能提高^[23]。

图 4 为 2 种熔覆层的 X 射线衍射图谱。由图 4 可见, 2 种熔覆层在 44.7° 、 65.0° 、 82.3° 处均出现明显的衍射峰, 表明 2 种涂层均由相同物相 (α -Fe) 固溶体组成。两涂层结构相同, 具有相似的特性。由于未出现其他物相的衍射峰, 故而说明 Cr、Ni、V、Mn、Mo、Si 等少量合金元素固溶于 (α -Fe) 中。Cr 在粉末中的含量较高, 且室温下能替代 (α -Fe) 中的 Fe 原子形成无限置换固溶体, 故 (α -Fe) 固溶体以含 Cr 固溶体为主^[24]。

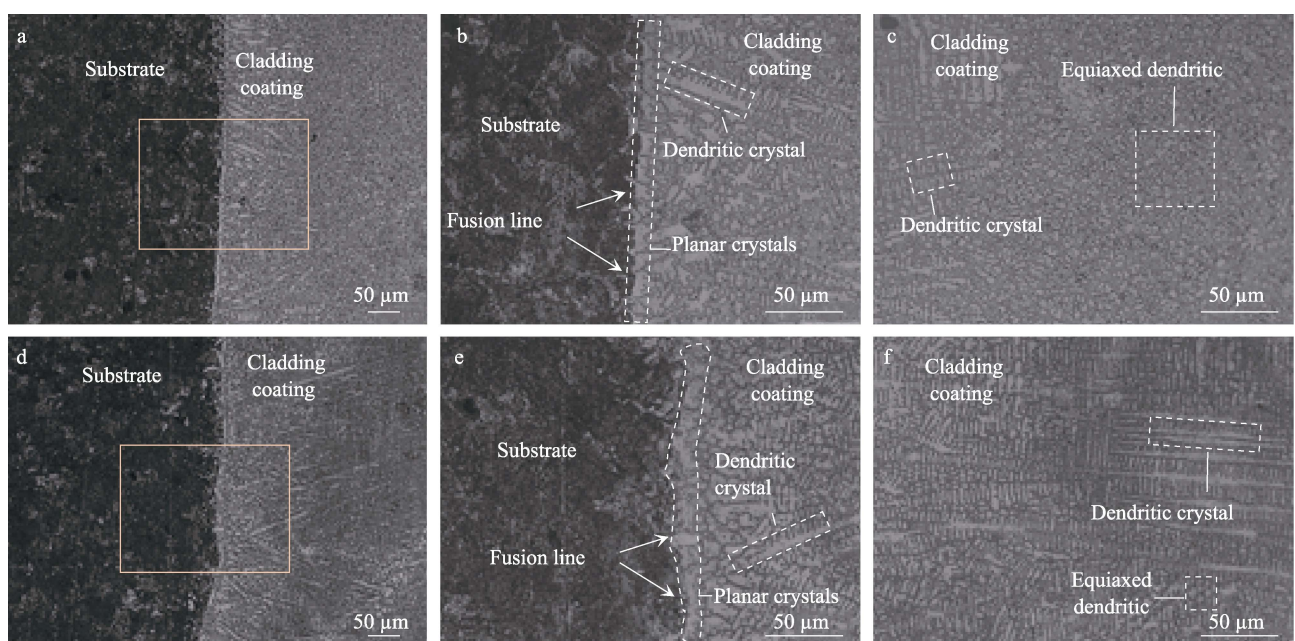


图 2 熔覆层的截面形貌: a~c) X_1 ; d~f) X_2

Fig.2 Cross-sectional morphologies of cladding coatings: a-c) X_1 ; d-f) X_2

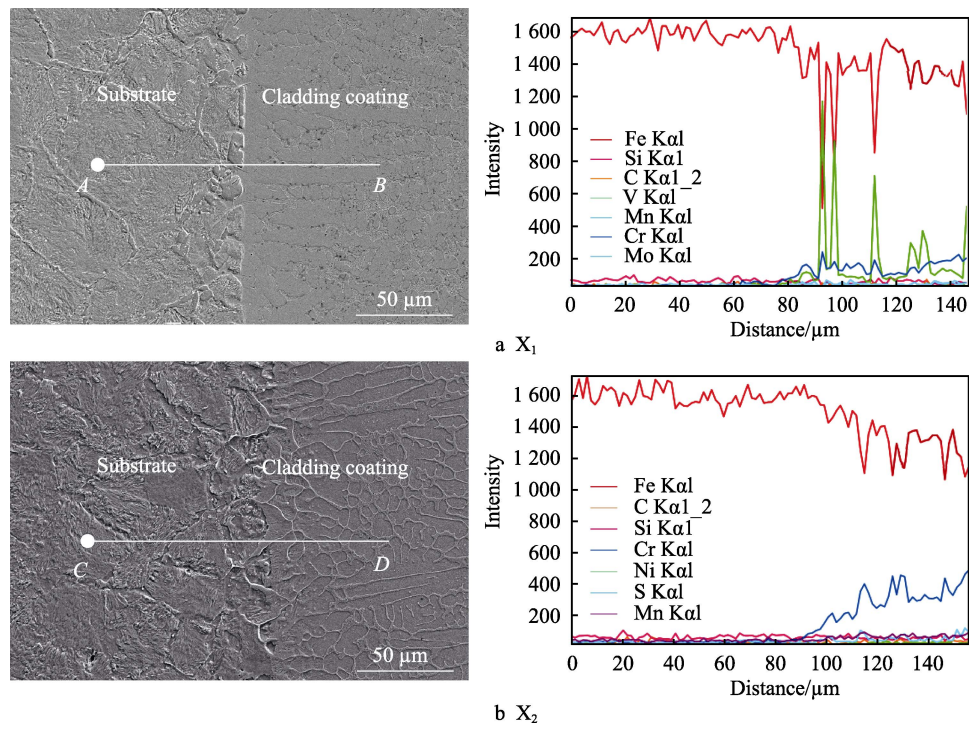


图 3 熔覆层与基体结合区的微观形貌和成分分布
Fig.3 Morphologies and composition distribution of the bonding zone between cladding coating and substrate

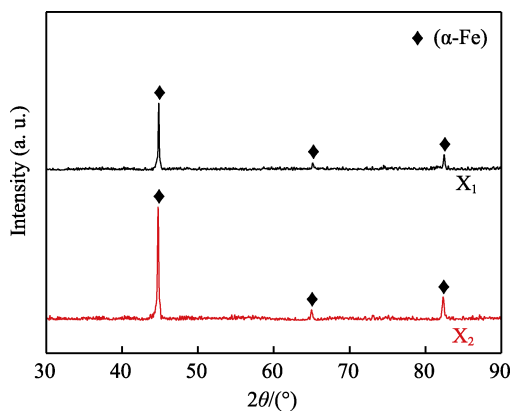


图 4 2 种熔覆层的 X 射线衍射图谱
Fig.4 X-ray diffraction patterns of two cladding coatings

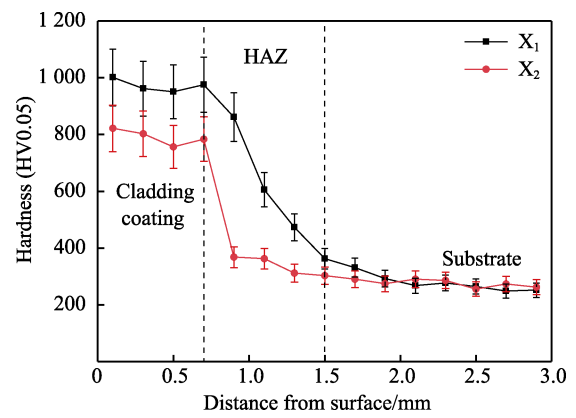


图 5 2 种熔覆层的硬度曲线
Fig.5 Hardness curves of two cladding coatings

2.4 结合区硬度分析

2 种熔覆层的截面硬度随距离变化曲线如图 5 所示。X₁ 熔覆层的硬度为 950~1 000HV，平均硬度为 975HV。X₂ 熔覆层的硬度为 784~821HV，平均硬度为 803HV。X₁ 熔覆层的平均硬度比 X₂ 熔覆层的硬度约高 21%，原因是 X₁ 熔覆层顶部含有大量细密的等轴晶组织。2 种熔覆层的外表面硬度最高，这与抗变形能力有关。凝固过程中，当固液界面推进到接近熔覆层表面时，此时 G/R 很小，结晶速度很快，组织向细小的等轴晶转变，晶界面积相对较大，由于晶界两侧晶体取向不同，晶界的高阻力使得塑性变形很难通过晶界从一个晶粒到另一个晶粒^[25-26]。图中 HAZ 为

热影响区，其硬度介于熔覆层和基体之间，原因是该区域中基体吸收部分能量发生微溶，使得热影响区少量晶粒粗化，另一个原因是熔覆层材料与基体材料混合引起的稀释作用^[27-28]。

2.5 熔覆层耐磨损性能分析

图 6 为 2 种熔覆层和 60Si2Mn 钢基体经过球-盘磨损试验后的微观形貌。通过观察磨痕宽度可以明显发现，X₁ 熔覆层的磨损程度最轻（图 6a），60Si2Mn 钢基体的磨损程度最严重（图 6c），而 X₂ 熔覆层的磨损程度介于二者之间。由此可见，X₁ 熔覆层的耐磨损性能最好。

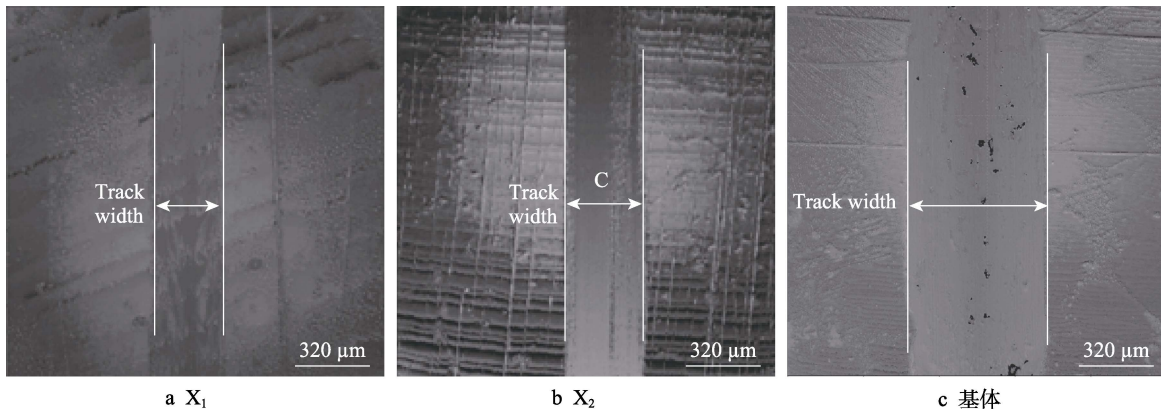


图 6 2 种熔覆层和 60Si2Mn 钢基体磨损后的微观形貌

Fig.6 Morphologies of worn surfaces of two cladding coatings and 60Si2Mn steel substrate: a) X₁; b) X₂; c) substrate

此外, 通过式 (1) 和式 (2) 可计算 2 种熔覆层和基体的体积磨损率, 通过对比体积磨损率数值大小也可确定其耐磨损性能。

$$W_v = \frac{\Delta V}{Fvt} \quad (1)$$

$$\Delta V = S \times L \quad (2)$$

式中: W_v 为体积磨损率, $\text{mm}^3/(\text{N} \cdot \text{m})$; ΔV 为体积磨损量, mm^3 ; F 为法向载荷, N ; v 为磨损速度, mm/s ; t 为磨损时间, s ; S 为磨损面积, mm^2 (可通过 Origin 软件数据处理获得); L 为振幅即磨损距离, mm 。

将表 4 中的摩擦磨损试验参数整理并代入体积磨损率公式中, 得到 X₁、X₂ 熔覆层以及基体的体积磨损率如图 7 所示。由图 7 可知, 3 种样品的体积磨损率分别为 1.32×10^{-4} 、 1.94×10^{-4} 、 $3.29 \times 10^{-4} \text{ mm}^3/(\text{N} \cdot \text{m})$ 。其中 X₁ 熔覆层的体积磨损率最小, 因此其耐磨损性能最好。

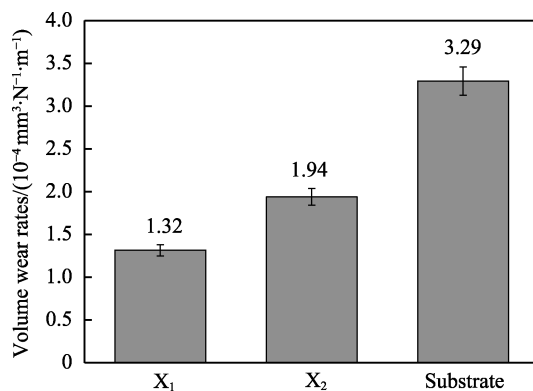


图 7 熔覆层和基体的体积磨损率

Fig.7 Volume wear rates of cladding coatings and substrate

3 结论

1) 2 种熔覆层均无裂纹、气孔等缺陷, 内部均由大量树枝晶、等轴晶和少量沿基材表面生长的平面晶构成, 其中 X₁ 熔覆层表面的等轴晶数量较多, 组织更均匀细小。原因是 X₁ 粉末中强碳化物形成元

素 V 含量较高, 易形成尺寸为纳米级的碳化物, 在晶界处阻碍晶粒长大, 起到细晶强化的作用。2 种熔覆层均由相同物相 ($\alpha\text{-Fe}$) 固溶体组成, 未出现明显的其他物相的衍射峰。

2) 2 种熔覆层的硬度和耐磨损性能均优于基体。基体 60Si2Mn 钢的平均硬度约为 300HV, X₁ 和 X₂ 熔覆层的平均硬度分别为 975HV 和 803HV, X₁ 熔覆层的硬度比 X₂ 熔覆层的硬度约高 21%。X₁ 熔覆层、X₂ 熔覆层以及基体材料的体积磨损率分别为 1.32×10^{-4} 、 1.94×10^{-4} 、 $3.29 \times 10^{-4} \text{ mm}^3/(\text{N} \cdot \text{m})$, 其中 X₁ 熔覆层的体积磨损率最小, 耐磨损性能最好。

参考文献:

- [1] 宋月鹏, 王伟, 高东升, 等. 基于表面工程技术制备农机刀具的研究现状[J]. 中国农机化学报, 2018, 39(1): 27-31.
SONG Y P, WANG W, GAO D S, et al. Research Status of Agricultural Machine Cutting Tools Treated by Surface Engineering Technology[J]. Journal of Chinese Agricultural Mechanization, 2018, 39(1): 27-31.
- [2] GUAN C S, FU J J, CUI Z C, et al. Evaluation of the Tribological and Anti-Adhesive Properties of Different Materials Coated Rotary Tillage Blades[J]. Soil and Tillage Research, 2021, 209: 104933.
- [3] GUAN C S, FU J J, XU L, et al. Study on the Reduction of Soil Adhesion and Tillage Force of Bionic Cutter Teeth in Secondary Soil Crushing[J]. Biosystems Engineering, 2022, 213: 133-147.
- [4] 蒋三生, 张新. 表面处理提高旋耕刀耐磨性研究现状[J]. 安徽农业科学, 2020, 48(1): 27-29.
JIANG S S, ZHANG X. Research Status on Surface Treatment to Improve Wear Resistance of Rotary Blade [J]. Journal of Anhui Agricultural Sciences, 2020, 48(1): 27-29.
- [5] 郝建军, 杨泽宇, 马路萍, 等. Fe-Cr-C-V 等离子堆焊层改善旋耕刀耐磨性和冲击韧性[J]. 农业工程学报, 2019, 35(3): 24-30.

- HAO J J, YANG Z Y, MA L P, et al. Fe-Cr-C-V Plasma Surfacing Layer Improving Wear Resistance and Impact Toughness of Rotary Blade[J]. Transactions of the Chinese Society of Agricultural Engineering, 2019, 35(3): 24-30.
- [6] BENEGRA M, SANTANA A L B, MARANHO O, et al. Effect of Heat Treatment on Wear Resistance of Nickel Aluminide Coatings Deposited by HVOF and PTA[J]. Journal of Thermal Spray Technology, 2015, 24(6): 1111-1116.
- [7] KAROONBOONYANAN S, SALOKHE V M, NIRANATLUMPONG P. Wear Resistance of Thermally Sprayed Rotary Tiller Blades[J]. Wear, 2007, 263(1/2/3/4/5/6): 604-608.
- [8] NIRANATLUMPONG P, SUKHONKET C, NAKNGO-ENTHONG J. Wear Resistant Surface Treatment of Pulverizer Blades[J]. Wear, 2013, 302(1/2): 878-881.
- [9] JU J, ZHOU Y, KANG M D, et al. Optimization of Process Parameters, Microstructure, and Properties of Laser Cladding Fe-Based Alloy on 42CrMo Steel Roller[J]. Materials, 2018, 11(10): 2061.
- [10] WANG K, ZHANG Z, XIANG D, et al. Research and Progress of Laser Cladding: Process, Materials and Applications[J]. Coatings, 2022, 12(10): 1382.
- [11] 张津超, 石世宏, 龚燕琪, 等. 激光熔覆技术研究进展[J]. 表面技术, 2020, 49(10): 1-11.
ZHANG J C, SHI S H, GONG Y Q, et al. Research Progress of Laser Cladding Technology[J]. Surface Technology, 2020, 49(10): 1-11.
- [12] 余敏, 张鸿羽, 曹开, 等. 激光熔覆在高速列车上的应用研究现状[J]. 表面技术, 2020, 49(10): 12-20.
YU M, ZHANG H Y, CAO K, et al. Application Status of Laser Cladding in High-Speed Trains[J]. Surface Technology, 2020, 49(10): 12-20.
- [13] 张玉杰, 杨建华, 许玲萍. 激光熔覆技术在表面失效机械件中的应用[J]. 电镀与精饰, 2021, 43(8): 39-43.
ZHANG Y J, YANG J H, XU L P. Application of Laser Cladding Technology in Mechanical Parts with Surface Failure[J]. Plating and Finishing, 2021, 43(8): 39-43.
- [14] 沈俊萍, 董景隆, 高红东, 等. 大型颚式破碎机偏心轴激光熔覆再制造技术研究[J]. 水泥, 2020(11): 55-59.
SHEN J P, DONG J L, GAO H D, et al. Research on Laser Cladding Remanufacturing Technology of Eccentric Shaft of Large Jaw Crusher[J]. Cement, 2020(11): 55-59.
- [15] TANIGAWA D, ABE N, TSUKAMOTO M, et al. The Effect of Particle Size on the Heat Affected Zone during Laser Cladding of Ni-Cr-Si-B Alloy on C45 Carbon Steel[J]. Optics and Lasers in Engineering, 2018, 101: 23-27.
- [16] ZHANG H, LIAN G F, ZHANG Y, et al. The Influence of Powder Size on the Microstructure and Properties of Mo_2FeB_2 Coating Fabricated via Laser Cladding with Pre-Placed Powder[J]. The International Journal of Advanced Manufacturing Technology, 2022, 120(9): 6041-6052.
- [17] 张磊, 陈小明, 苏建灏, 等. 激光熔覆 Fe-Mo-V-C 合金涂层组织及摩擦磨损性能[J]. 粉末冶金材料科学与工程, 2020, 25(1): 65-71.
ZHANG L, CHEN X M, SU J H, et al. Microstructure and Frictional Wear Performance of Fe-Mo-V-C Alloy Coating Prepared by Laser Cladding[J]. Materials Science and Engineering of Powder Metallurgy, 2020, 25(1): 65-71.
- [18] 李聪玮, 刘泽, 王明, 等. 铁基激光熔覆层的微观结构和摩擦磨损性能研究[J]. 矿冶工程, 2021, 41(5): 149-152.
LI C W, LIU Z, WANG M, et al. Microstructure, Friction and Wear Properties of Iron-Based Laser Cladding Coating[J]. Mining and Metallurgical Engineering, 2021, 41(5): 149-152.
- [19] GUO W, ZHANG L P, XU C, et al. Study on the Wear Resistance of Laser Cladding Iron-Base Alloy by Heat Treatment[J]. Materials Research Express, 2018, 6(2): 026572.
- [20] GUO W M, LI X Q, DING N, et al. Microstructure Characteristics and Mechanical Properties of a Laser Cladded Fe-Based Martensitic Stainless Steel Coating[J]. Surface and Coatings Technology, 2021, 408: 126795.
- [21] 叶四友, 刘建永, 杨伟. 激光熔覆 316L 不锈钢涂层组织和性能的研究[J]. 表面技术, 2018, 47(3): 48-53.
YE S Y, LIU J Y, YANG W. Microstructure and Properties of Laser Cladded 316L Stainless Steel Layer[J]. Surface Technology, 2018, 47(3): 48-53.
- [22] OUYANG C Y, BAI Q F, YAN X G, et al. Microstructure and Corrosion Properties of Laser Cladding Fe-Based Alloy Coating on 27SiMn Steel Surface[J]. Coatings, 2021, 11(5): 552.
- [23] 田玉亮, 李杰. Cr 含量对铁基激光熔覆层组织与性能的影响[J]. 矿冶, 2020, 29(6): 74-79.
TIAN Y L, LI J. Effect of Cr Content on the Structure and Properties of Fe-Based Laser Cladding Layers[J]. Mining and Metallurgy, 2020, 29(6): 74-79.
- [24] CHEN J L, ZHOU Y J, SHI C, et al. Microscopic Analysis and Electrochemical Behavior of Fe-Based Coating Produced by Laser Cladding[J]. Metals, 2017, 7(10): 435.
- [25] 张华健, 孙中刚, 李峰, 等. 激光熔覆铁基复合涂层组织与性能影响[J]. 表面技术, 2018, 47(12): 127-133.
ZHANG H J, SUN Z G, LI F, et al. Effect of Microstructure and Properties of Laser Cladding Iron-Based Composite Coatings[J]. Surface Technology, 2018, 47(12): 127-133.
- [26] HUANG F X, JIANG Z H, LIU X M, et al. Effects of Process Parameters on Microstructure and Hardness of Layers by Laser Cladding[J]. ISIJ International, 2011, 51(3): 441-447.
- [27] BAI Q F, OUYANG C Y, ZHAO C J, et al. Microstructure and Wear Resistance of Laser Cladding of Fe-Based Alloy Coatings in Different Areas of Cladding Layer[J]. Materials, 2021, 14(11): 2839.
- [28] 尹燕, 潘存良, 赵超, 等. 激光熔覆高铬铁基合金的组织形成机制及对显微硬度的影响[J]. 焊接学报, 2019, 40(7): 114-120, 166.
YIN Y, PAN C L, ZHAO C, et al. Formation Mechanism of Microstructure of Laser Cladding High Chromium Fe-Based Alloy and Its Effect on Microhardness[J]. Transactions of the China Welding Institution, 2019, 40(7): 114-120, 166.